Stability and Redispersion of Ni nanoparticles supported on N-doped carbons for the CO_2 electrochemical reduction

Paulina Prslja, Núria López [*]

Institute of Chemical Research of Catalonia, ICIQ, The Barcelona Institute of Science and Technology, Av. Països Catalans, 16, 43007 Tarragona, Spain

Abstract

N-doped carbon systems constitute a unique platform for the isolation of metal atoms that have been proposed as active species in the electrocatalytic CO_2 reduction reaction (eCO_2RR). Among them the Nickel Nitrogen Carbon (NiNC) single-atom catalyst exhibits the highest efficiency for producing CO, at different potentials. The variation in the material synthesis produces defects with coordinatively saturated and unsaturated N-doped cavities, and once the metal is placed there these single atoms can present different metal oxidation states depending on the cavity nature. Synthetic protocols to produce single atoms from metal nanoparticles have been put forward, then the so-synthetized materials are complex as contain a variety of metal environments. Thus, although many studies have been devoted to NiNC materials, there are still discussions on the true nature of the active sites and particularly their coordination environment. In the present work, we have computationally evaluated experimental activity and selectivity of a wide potentially active sites for the single atoms and nanoparticles, where the optimal reactivity is found for N-doped models. The second aspect addressed here concerns the electrochemical stability of the reconstruction and redispersion of supported nanoparticles. At high CO coverages, Ni nanoparticles reconstruct by forming $Ni(CO)_4$ species that can redisperse on the host into active single atoms. In summary, the complexity of these metal-doped carbon systems needs to be considered holistically to understand their real electrocatalytic behavior.

KEYWORDS: electrocatalytic CO_2 reduction, NiNC catalyst, single-atom catalyst, reconstruction of Ni nanoparticles

1. Introduction

Single Metal Nitrogen Carbon materials (M-N-C) have been proposed as one of the most attractive catalysts for electrocatalytic CO_2 reduction reaction (eCO_2RR). Furthermore, with maximum atom efficiency and low coordination metal centers, they show high selectivity towards producing CO[1–4] even with competing hydrogen evolution reaction (HER). Combined products or syngas can be used to produce liquid hydrocarbons via Fischer-Tropsch synthesis. Moreover, the M-N-C materials can further reduce CO to hydrocarbons.[3,5,6] The experimentally most studied example of these types of materials, even proposed to be industrially efficient, come from Ni-N-C, which is highly selective to producing CO.[7–20]

The efficiency of those materials can be controlled by synthetic and post-synthetic treatments. Their nitrogen content can be controlled in several ways, such as changing the doping temperature[20]. All these approaches change the nature of the cavities present both in terms of size and coordination environment. Therefore, we can classify the hosts according to these cavities as saturated and unsaturated N-doped carbon materials. Homogenous-like confinement of the metal in the cavities plays an important role in preventing the migration as the material goes through high-temperature carbonization.[21] The vacancies can be synthetically tailored by employing MOF scaffolds,[4,22] by oxidizing carbon materials and further doping with nitrogen to form undefined motifs,[20,23] and by depositing porphyrin-like complexes.[5,24–26] The ultimate (i) size and structure of the defect in which the metal is embedded; (ii) the nitrogen content which can be controlled with the doping temperature[20] and (iii) the reaction conditions determine the nature of the metal sites, their coordination environment, and the size of the metal nanoparticles thus affecting the electronic structure of the active metal. Targeting activity and selectivity require adapting the anchoring sites to the metal electronic properties so that they can synergistically act.

To understand the efficiency and selectivity of the materials, different types of catalysts were synthesized and tested under electrochemical eCO_2RR.[20] To be concrete, (i) Ni nanoparticles supported on carbon material, (ii) single metal atom in saturated N-doped carbon material, (iii) sample containing both particles and single atoms, and (iv) Ni nanoparticles supported on unsaturated N-doped carbon materials. Importantly, significant changes in efficiency and product distribution were observed when repeating the electrochemical reaction five times in a row. This effect was particularly acute for the Ni-containing colloidal nanoparticle samples on the unsaturated N-doped materials. With the colloidal particle method, the size and particle loading can be controlled, and this preparation method is crucial for the stability of the catalyst

and depends on the support. High efficiency can also be seen in the Ni single atoms induced by thermal atomization in N-doped carbon but it does not occur over pure carbon support.[19] Ni particles and Ni single active sites supported on carbon nitrides[27] featured high selectivity towards CO. These authors demonstrated that the materials can boost the conversion of CO_2 into CO.[10] All these works highlight the role of the nature of the support and how its detailed characterization allows to fine tune the chemical properties of these materials.

To shed light and rationalize such catalytic behavior, we turn to computational simulation at the atomic level of detail. In the present work, we explore different N-doped carbon materials, both saturated and unsaturated, as reported in previous experiments.[20] We then compute the activity of Ni catalysts for eCO_2RR, both as a nanoparticle and as single atoms embedded in different coordination environments. Furthermore, we report a model nanoparticle to link the possible redispersion and reconstruction under electrochemical conditions when being supported on unsaturated N-doped carbon materials.

Computational details

All simulations were performed using spin-polarized Density Functional Theory (DFT) as implemented in the Vienna Ab initio Simulation Package (VASP)[28,29] using the GGA PBE-D3 density functional.[30,31] Core electrons were described by projector augmented wave (PAW)[29,32] while valence electrons were expanded by plane wave basis sets with a kinetic energy cut-off of at least 500 eV.

N-doped carbon materials are represented with a graphene layer expanded in a (6×6) supercell and replacing carbon atoms by nitrogen atoms to design saturated and unsaturated N-doped carbon models. These layers were interleaved by 12 Å vacuum along the z direction. A nickel atom was placed in the cavity left on the carbon sheet. Structures were relaxed with a force threshold of 0.050 eV/Å. The Brillouin zone was sampled using a (3×3×1) *k*-point mesh generated with the Monkhorst–Pack method.[33]

Ni nanoparticles were represented using three metal surfaces with the lowest Miller indexes (and thus lowest surface energies) Ni(100), Ni(111), and Ni(211). High quality surface energy calculations ((10×10×1) *k*-point mesh) were performed to build the nanoparticle structure using the Wulff model[34,35] with VESTA.[36] The vacuum between slabs was larger than 10 Å and the

structures were relaxed with a force threshold of 0.025 eV/Å. They contained five layers, where the two uppermost were fully relaxed and the rest were fixed to the bulk structure.

CO can adsorb in very dense phases on Ni[37,38] thus different coverages were considered: from 1/12 to 12/12 ML for Ni(100) and Ni(211) and from 1/16 to 16/16 ML for Ni(111). The Brillouin zone was sampled using a (3×4×1), (3×3×1), and (5×3×1) *k*-point meshes for Ni(100), Ni(111), and Ni(211) respectively. The Wulff construction was also employed on the CO-dense phases to explain the restructuring of the nanoparticles. $Ni(CO)_x$ species can be formed in rich CO environments, which can then redisperse and reconstruct the Ni nanoparticle. The Ni(211) surface edge has enough space to accommodate more than one CO molecule, allowing the formation of $Ni(CO)_4$ complexes. We thus calculated the formation and elimination of $Ni(CO)_4$ with different CO coverages on that surface, where the elimination of this species forms a vacancy at the edge of the Ni(211) steps. The $Ni(CO)_4$ formation enthalpy computed with PBE starting from CO is more exothermic than the experimentally reported, the implications for this deviation are evaluated in the text.

For all the systems described before, we obtained the energies of the relevant intermediates in the electrochemical environment under eCO_2RR conditions by considering the computational hydrogen electrode (CHE).[39,40] The intermediates energies were corrected with calculated zero point and entropic contributions. Notice that for the first step where CO_2 adsorbs on the metals it drags charge from the system, the notation then implies that it is activated, and the calculations were done in boxes with zero net charge. Gas-phase molecules used as a reference were calculated with PBE functional. Zero-point, entropic, and heat capacity contributions are shown in Table S1.[41] Solvation effects were added to CO and COOH intermediates following the values employed in ref. [41]. We have tested and compared the results of our in-house implicit solvent model (VASP-MGCM)[42] to the values in the literature, Table S5-S6. Solvation of N-doped carbon systems are known to depend on the N-concentration and we have evaluated these effects in our case. [43] However, in our models the N-doping occurs close to a single point in the cavity and thus the effect by changing the stoichiometry of the cavity is reduced, for the NiN_3 and NiN_4 models -0.39 and -0.35 eV, respectively. Further details on thermodynamic corrections are discussed in the Supporting Information. All structures can be retrieved from the database ioChem-BD[44] via the following link[45], which contains a unique and labeled list of the DFT calculations of this project.

Results and Discussion

1. Computational characterization of the materials.

To understand the selectivity and activity of N-doped or N-free carbon materials, we modeled them under reaction conditions. The DFT simulations were performed on several N-doped defects where the Ni atoms can be anchored, as well as Ni nanoparticles can be supported, to represent the species characterized in experiments.[20] In **Figure 1** we show three families of models: (a) saturated N-doped carbon materials (NiN_xC) representing NiN_4 and similar undefined N-doped materials made at low doping temperature, (b) unsaturated N-doped ($NiNC_x$) and N-free materials (NiC_x) typically occurring for carbons at high doping temperatures, when the nitrogen content decreases, and (c) Ni metal surfaces composing the supported nanoparticles on the unsaturated N-doped supports (Ni_{NP}-NC_x). This approximation allows us to provide a holistic chain of models that accounts for the complexity of the N-doped carbon support and the metallic nature of the nanoparticle. The ultimate aim is to show the role of the speciation (charge, oxidation state, and coordination environment) on the electrochemical activity and the dynamic behavior or the different synthetic preparations. We simulated EXAFS spectra for all catalysts (**Figure S1**), where NiN_xC (saturated N-doped materials) agreed well with experimental data.[20] DFT structural parameters are presented in **Table S4**.

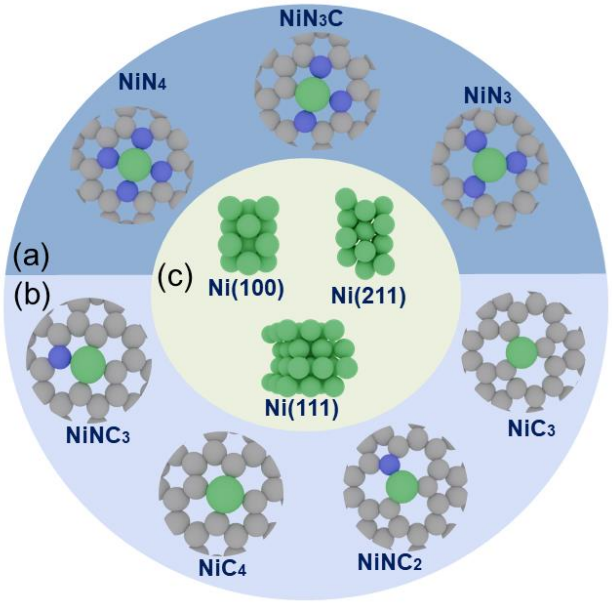

Figure 1. Computational models for different systems. (a) Saturated N-doped carbon material. (b) Unsaturated N-doped or N-free carbon material. (c) Metal surfaces. C in grey spheres, N in blue, and Ni in green.

2. Activity and selectivity of the materials.

The activity and selectivity of the modeled catalysts can be discussed in terms of the corresponding Gibbs free energy profiles, presented in **Figure 2**. The electrochemical activity was analyzed by calculating the binding energies of the intermediates according to the most agreed mechanism for CO_2 to CO reduction (**Figure 2a–c**). The process requires only a 2 electron transfer and the steps are: (i) $CO_2 + e^- \rightarrow *CO_2$, (ii) $*CO_2 + H^+ \rightarrow *COOH$ (also, the first two steps in the literature are combined into: $CO_2 + H^+ + e^- \rightarrow *COOH$), (iii) $*COOH + H^+ + e^- \rightarrow *CO + H_2O$ and (iv) $*CO \rightarrow CO_{(g)} + *$. Notice that once CO_2 is adsorbed, activated, and polarized with partial charge transfer (see **Table S10**) from the host material and thus step (i) does not correspond to any extra electron added to the simulation box.

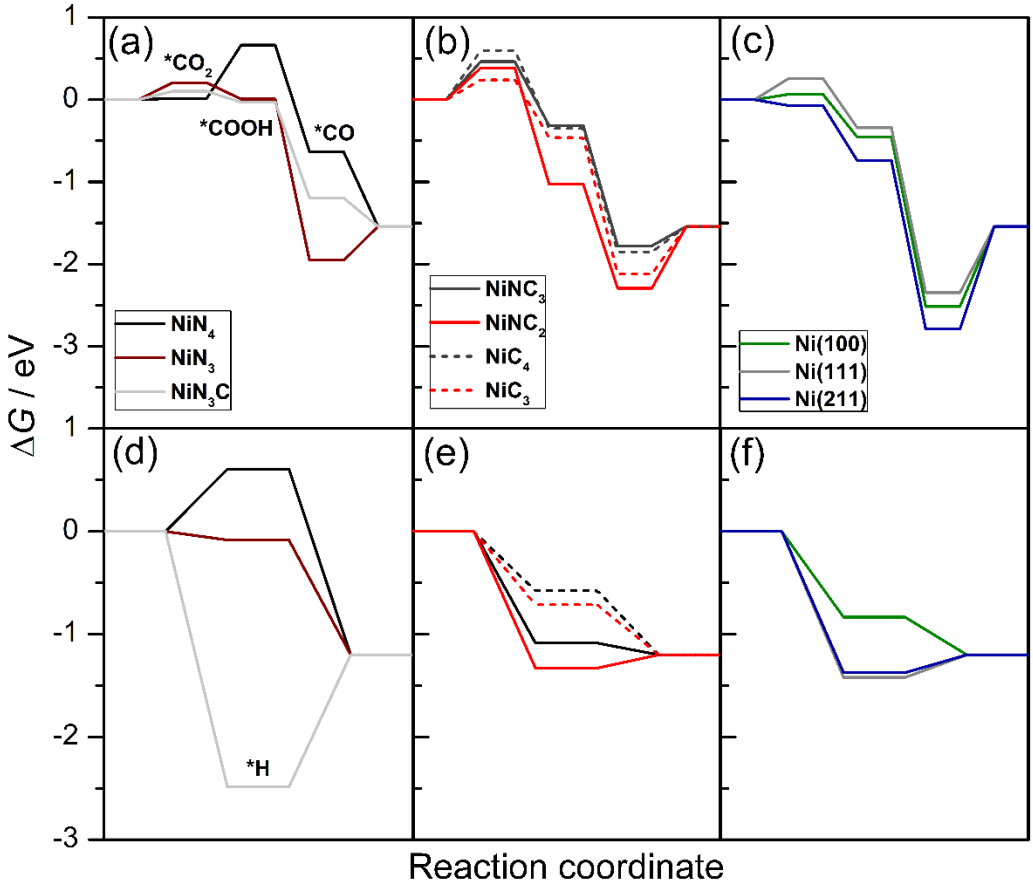

Figure 2. Gibbs free energy profiles for (a, b, and c) eCO_2RR and (d, e, and f) HER over different model sites at U = −0.6 V *vs.* RHE (for reference the experimental pH was 7). (a,d) Saturated nitrogen-doped carbon materials. (b,e) Unsaturated or free N-doped carbon materials. (c,f) Metal surfaces.

In agreement with the previous results, we can see that the highest activity towards CO is shown by unsaturated N-doped materials[7] and metal surfaces, as they bind CO strongly. Regarding the selectivity, it can be discussed by comparison to the competing HER **(Figure 2d–f)**. Saturated N-doped materials reach the highest selectivity towards CO, where NiN_4 and NiN_3 are representative models, while NiN_3C model binds *H strongly. Therefore, based on the experimental selectivity[20] of single-atom catalysts the NiN_3C model is not representative. For a catalyst to be selective towards CO, the binding of *COOH and $*CO_2$ intermediates need to be strong to reduce the onset potential. Also, selectivity can be compared with *H binding energy and CO desorption energy. The correlation between the adsorption energies of *COOH and *H is shown in **Figure 3a.** We can see that NiN_4 and NiN_3 bind *H weakly, therefore saturated N-doped materials are selective. NiN_4 binds $*CO_2$ and *COOH weakly, which means it has a higher onset potential, while the opposite trend is seen for NiN_3. The computed onset potentials are presented in **Table S11**, where NiN_3 has a lower onset potential than NiN_4 because it binds *COOH stronger. Ni(211) and $NiNC_2$ bind strongly *H and *COOH, which means they will not be selective toward CO. Ni(100) would be the best candidate among the metal surfaces as it binds *H weakly and *COOH relatively strongly. **Figure 3b** represents a correlation between adsorption energies of $*CO_2$ and desorption of CO, where CO_2 activation can relate to Bader charges of the adsorbed CO_2 molecule (see **Table S10**). NiN_3, $NiNC_3$, and Ni(100) bind $*CO_2$ relatively strong, where Ni(100) binds *CO strongly (see **Figure S3**), which means the rate of CO formation would be low. The strong adsorption energy of *H for Ni(100) and $NiNC_3$ can be related to low selectivity, where HER and eCO_2RR compete. The most interesting system is NiN_3, because of the optimal *CO binding and the weakly *H binding. From an electronic structure point of view, the Ni atom in the NiN_4 square planar confinement is in the Ni^{2+} oxidation state, while that in the NiN_3 trigonal planar configuration is in the Ni^{+} oxidation state (see **Figure S4**). This special role of Ni^{+} is long known in organometallic chemistry[46] and even in thermal catalysis.[47] The change in the oxidation state has an impact on the geometries of the activated CO_2 intermediate as both the O-C-O angle and Ni-C(CO_2) distance indicate the degree of activation of the CO_2 molecule in the N-doped saturated materials. In **Figure S5**, the linear scaling relationship of CO_2 geometry and adsorption of *CO shows that the activation in NiN_3 correlates with the medium binding of *CO, while the lowest activation appears in NiN_4 with a C-O-O angle of 170.2º. All these fingerprints point out the relevance of understanding the organometallic structures when trying to identify the most suitable defects for a given metal and the importance of the charge state for the encapsulated metal ions.

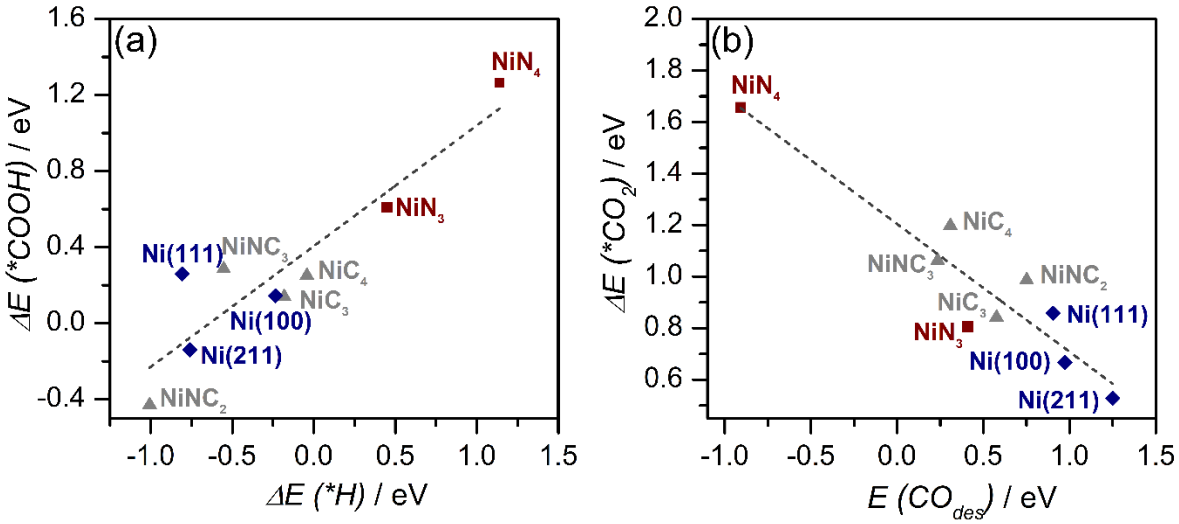

Figure 3. Linear scaling relationship. (a) Linear COOH binding energy scaling relations for adsorption of H atom. (b) CO_2 binding energy and corresponding linear-scaling relationships for desorption of CO molecule. Saturated N-doped carbon materials are represented with red symbols, unsaturated N-doped carbon materials with grey symbols, and metal surfaces with blue symbols.

3. Reconstruction of Ni NPs on N-doped carbon materials.

Electrocatalysts can be affected by the presence of different variables. In our case, the reconstruction of Ni NPs and the disintegration of $Ni(CO)_2$ complexes change the activity and selectivity. Once the reconstruction happens experimentally, the partial current density of H_2 drastically drops compared to that of CO, thus favoring the disintegration process. Such dynamic behavior of electrocatalysts is crucial for their performance and thus we here address these aspects by simplified models.

To investigate the role of the reaction products in the stability of the Ni NPs, we model a nanoparticle-based on the lowest-energy surfaces through a Wulff construction. This is straightforward for metal nanoparticles and can be extended when adsorbates, like CO, are present.[37,48] In addition, we apply the atomistic version of Ostwald ripening theory[49,50] by the formation of $Ni(CO)_2$ complexes to show when the disintegration of nanoparticles can occur on such N-doped carbon materials.

3.1. Nanoparticle shape

To address the role of nanoparticles we first focus on their structure. The size of the synthesized Ni NPs was 2.5 to 7 nm, and thus they can be represented via the Wulff construction that corresponds to the equilibrium structure for a medium-to-large nanoparticle and it is obtained from the surface energies. We calculated the surface energies for three orientations Ni(111), Ni(100), and Ni(211), and, employing the Wulff construction, we then extracted the corresponding areas for each facet. The average surface energy for the nanoparticle is 0.126 eV/Å. All surface energies and ratios of the corresponding facets are presented in **Table S17**.

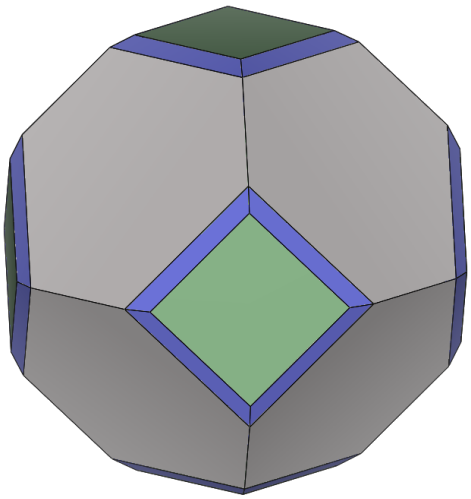

Figure 4. Wulff construction based on the surface energies calculated by DFT. Surface legend: Ni(100) in green, Ni(111) in gray, and Ni(211) in blue.

To assess the change in the nanoparticle-induced by the environment, we consider CO adsorption on all three facets separately.[37] We calculated average binding energies E'_{CO}, for a range of coverages 1/12 to 12/12 ML for Ni(100) and Ni(211) facets, and Ni(111) from 1/16 to 16/16 ML (**Figure S7**). In all cases, at low to medium coverages, all the modified surface energies (γ_x') are smaller, but the reduction in surface energies depends on the particular facet orientation. The detailed balance between adsorption sites and CO-CO repulsion contributes to the surface energy in a non-linear way, as to achieve higher CO densities the molecules need to go to rather unstable sites. At 0.25 ML we are left with Ni(100) and Ni(111) surfaces, while at full coverage of 1ML the extent of Ni(211) facet in the nanoparticle increases and Ni(111) reconstructs (see **Figure S6)**. In summary, the average surface energy for the decorated nanoparticle (γ') at CO coverage 0.25 ML is 0.095 eV/Å^2, which is 0.031 eV/Å^2 less than for

the bare one (**Table S16**). Therefore, the nanoparticle under product-rich conditions has more surface Ni atoms with less Ni-Ni average coordination. This could be the first step towards disintegration. In addition, this high product coverage influences the selectivity as it limits the HER reaction. The effect can be explained with the Gibbs free energies of the *H intermediate for the clean and on the CO covered (θ=0.92ML) Ni surfaces (see **Figure S10**). Once Ni surfaces are covered with CO, *H binds weaker (lowering the selectivity for HER), see **Figure S11**. This agrees with the experimental observations showing a drastic drop of H_2 partial current density. Thus, selectivity is triggered by minimizing the HER path.

3.2. Gibbs free energy of $Ni(CO)_x$ complexes disintegration on N doped carbon materials

We applied the energetic formalism from Ouyang and co-workers[50] to evaluate whether the disintegration of $Ni(CO)_x$ from Ni NPs is possible on N-doped carbon materials. We followed the criteria of reactant induced dynamics, where feasibility can be explained by the Gibbs free energy of disintegration (ΔG^{dis}_{NP}). First, we compute the formation energy of isolated metal adatom (E^f_{Ni}) with respect to Ni bulk reference supported on the different carbon defects (**Table S18**). From these results, we can see that formation energies are exothermic, as Ni atoms are anchored to a defect. Second, we calculate the Gibbs free energy for the CO-decorated nanoparticle, ΔG^{dis}_{NP}, following the equation:

$$\Delta G^{dis}_{NP}(R,T,p) = E^f_{surf\text{-}nCO} - n\times\Delta\mu_{CO}(T,p) - \Delta E'_{NP}(R) - TS \qquad \text{Eq. (1)}$$

Where, $E^f_{surf\text{-}nCO}$ is the energy of the Ni atom coordinated to the N-doped carbon substrate and n remaining CO molecules, $\Delta E'_{NP}(R)$ is the energy of the CO-covered nanoparticle with radius R, and $\Delta\mu_{CO}(T,p)$ is the excess chemical potential of CO (T, p). In our case, the configurational entropy S was not included because the number of cavities is difficult to assess; however, it will favor dispersed species. Therefore, the values obtained here for the transition correspond to a maximum threshold. The excess chemical potential was set to $\Delta\mu_{CO}(T,p) = -0.76$ eV[51] corresponding to experimental conditions of 300 K and 0.10 mbar. The binding energy of nCO (E^f_{1CO}) needs to be negative and lower than $\Delta\mu_{CO}(T,p) = -0.76$ eV. When both requirements are fulfilled, nanoparticle disintegration is thermodynamically possible.

The nature of the cavities in the support provides a large versatility regarding the stability against disintegration. In our investigations, we have considered all 7 types of defects in **Figure 1**. The anchored Ni atom in saturated N-doped models is coordinated either to pyridinic or

pyrrolic N atoms, which are strong ligands able to easily trap metal atoms. This is in line with experiments where they do not observe nanoparticles on those materials. We observe an opposite trend for the unsaturated N-doped materials, where Ni NPs can redisperse into single-atom cavities. The reason for that is the decreased N-content and increased C-content in the materials, which makes Ni dynamic and prone to aggregate and disintegrate in the presence of dense CO phases and electrochemical conditions. Therefore, single Ni metal atoms with little aggregation are expected in agreement with experiments.[10] Finally, we show that the redispersion of Ni NPs on NC_2 defect (unsaturated N-doped model) is thermodynamically possible. $NiNC_2$ is also one of the most active and non-selective eCO_2RR configurations, with strong bindings for *CO, *COOH, and *H intermediates. Once Ni NPs are supported on NC_2 they can disintegrate, as the experimentally partial current density drops drastically compared to CO partial current densities. That is how the combination of the two results (activity and stability for dispersion) can support the fact that enhanced Faradaic efficiency was observed when the reaction was performed five times in a row for nanoparticles supported on unsaturated N-doped carbon materials.[20] Redispersion is thus possible on unsaturated materials; however, depending on the nature of the carrier that would imply a different performance. As the performance of the single atoms depends on the properties of the cavity, redispersion would only be more favorable provided that the right cavity exists, and it is occupied. The electrochemical cycling from the nanoparticles does enhance the selectivity in unsaturated hosts but not up to the levels found for the saturated materials.

To investigate the size (R) dependence of the disintegration induced by CO, we have used Ni_{NP}-NC_2 as cavity and have calculated the $\Delta G^{dis}_{NP}(R, T, p)$ considering the formation of $Ni(CO)_2$ sitting at these pockets at experimental temperature and pressure. **Figure 5** presents the ΔG^{dis}_{NP} corresponding to $Ni(CO)_2$ versus the radius R of a Ni nanoparticle at two different coverages, 0.25 ML and 1ML (non-wetting conditions for the nanoparticle were considered, thus the Young angle was set to 180º). We found that ΔG^{dis}_{NP} decreases at smaller R and crosses the reference level (−2.7 eV, energy of an isolated Ni atom in the cavity) at about 40Å for 1 ML and 20Å for 0.25 ML. The lower value found for lower coverage is a direct consequence of the simplicity of the model and shall be taken with caution as kinetic constraints related to the need of concentrating CO molecules to extract the surface atoms could play an important role. At high coverage, our results imply that Ni NPs smaller than 4 nm will disintegrate into $Ni(CO)_2$ when supported on the NC_2 at 300 K and 0.1 mbar.

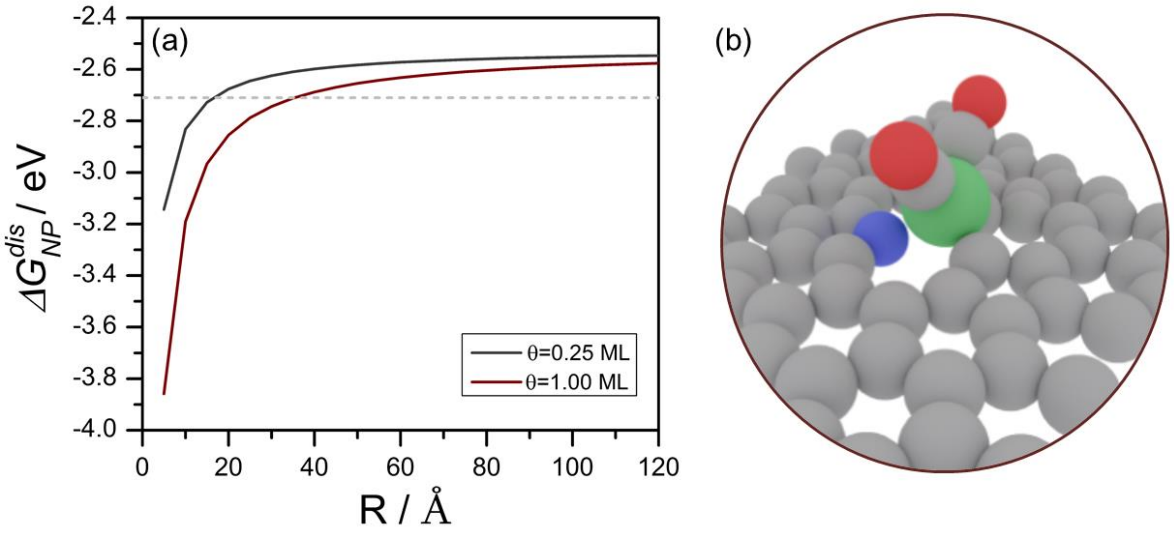

Figure 5. (a) Size dependence of the Gibbs free energy (ΔG^{dis}_{NP}) of $Ni(CO)_2$, when Ni_{NP} is supported on NC_2 at 300 K and 0.1 mbar. The horizontal dashed line indicates the limit for stability. (b) Schematic representation of $Ni(CO)_2$ bound to the NC_2 cavity.

3.3. The mechanism for Ni nanoparticle reconstruction.

The dense layers that we have identified in Section 3.1 show that after eCO_2RR, CO extensively covers the surface and over long times has the potential to increase the fraction of Ni atoms in low-coordinated sites as stepped Ni(211) surfaces. Moreover, the thermodynamic models in Section 3.2 indicate that below a certain size, $Ni(CO)_x$ clusters can be stable in some particular motifs of the N-doped carbons. To merge these two scenarios, a viable route for decomposition needs to be described. Ni can form volatile species with CO in the form of $Ni(CO)_4$ that can be soluble under the reaction conditions. We have calculated the energy needed for the formation of these species.

On nanoparticles, CO_2 is reduced to CO at −0.6 V vs. RHE and pH 7, and the resulting CO drives the reconstruction toward Ni(211). Once the reaction is stopped at open circuit potential (OCP), $Ni(CO)_4$ species can be formed as the CO coverage is very high. Thermodynamically, the formation energy of a metal vacancy (with respect to Ni bulk) in Ni(100), Ni(111), and Ni(211) surfaces are 0.59, 1.04, and 0.33 eV, respectively. Strong kinetic limitations can likely appear due to geometric constraints on Ni(111) and Ni(100), but for the fully CO adsorbed Ni(211) surface the step edges can present very high CO concentration. Thus $Ni(CO)_4$ can be formed in this face with concomitant elimination of Ni atoms. **Figure 6a** presents the average

adsorption energy for CO at different coverages (red curve) on the Ni(211) facet and it is compared to the formation-elimination of the $Ni(CO)_4$ complex (gray curves). The crossing between these two lines can be interpreted as the coverage at which the elimination of Ni atoms in the form of the species becomes viable. Therefore, high CO coverages would affect the stability of the edge sites starting around 0.78 ML coverage (when using DFT or experimental value for $Ni(CO)_4$) promoting the formation of the species that can then redisperse on the cavities of the N-doped carbon. The process of reconstruction is sketched in **Figure 6b**. All the data is presented in **Tables S21–23**. Once the reaction is under electrochemical potential again, these complexes react with non-occupied defects on the unsaturated N-doped carbon (Ni_{NP}-NC_2) and effectively redisperse. This process could potentially lead to higher activity, as shown in the experiments.[20]

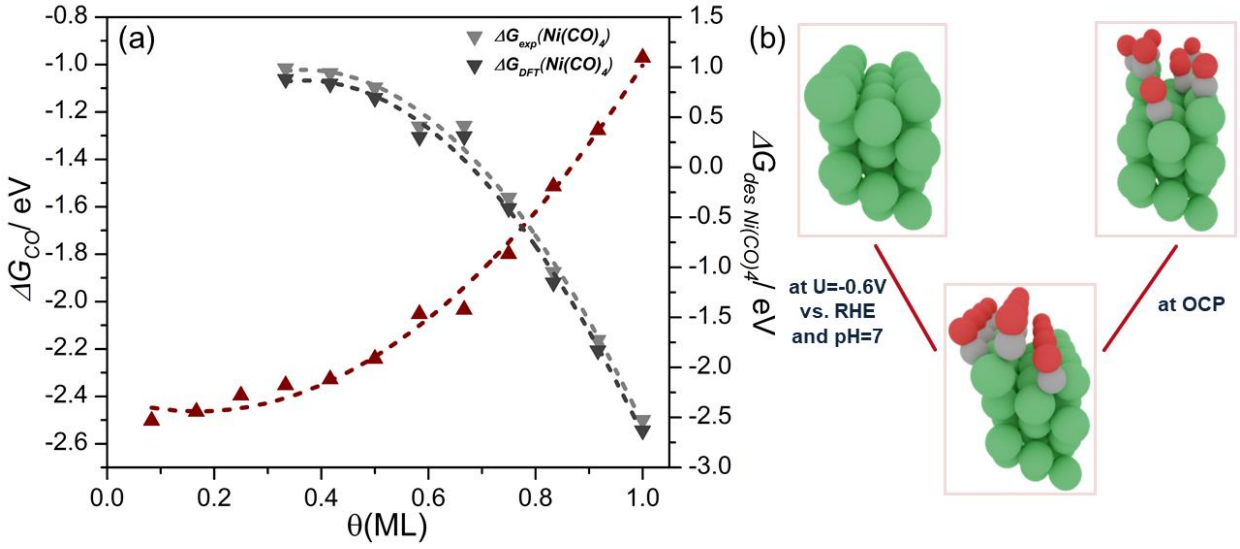

Figure 6. Process of Ni(211) metal surface reconstruction. (a) CO coverage dependence of the average Gibbs free energy (red curve) of CO adsorption at U = −0.6 V *vs.* RHE (pH = 7) and (gray curves) desorption of $Ni(CO)_4$. (b) Schematic process of clean Ni(211) metal surface fully adsorbing CO at electrochemical conditions. When the reaction is stopped at the open circuit potential (OCP) to assess the material recyclability, $Ni(CO)_4$-like complexes can desorb.

Conclusions

Electrocatalysts based on Ni supported on N-doped carbon materials have been computationally analyzed for the reduction of CO_2 considering both nanoparticles and single atoms. The optimal activity and selectivity are found for NiN_3 model, in which Ni is in Ni^{1+} oxidation state. NiN_3

exhibits theoretically low onset potential in agreement with experiments and high rate towards CO. However, rather saturated N-doped materials are more selective towards CO formation. As single atoms can be prepared from nanoparticles, we show through the Oswald formalism that disintegration of $Ni(CO)_x$ can happen if Ni nanoparticles are supported on N-doped unsaturated support such as NC_2. We present a mechanism of Ni(211) surface reconstruction that is possible only at high CO coverages around 8/12 ML by the formation of $Ni(CO)_4$ species, which then redisperse into active single atoms. The complete understanding of the Ni-N-C materials points towards a very dynamic behavior where considering the full complexity of the material in terms of Ni nuclearity and environment is needed. This is likely a common feature for such type of electrocatalysts.

Funding Sources

ELCOREL, European Union's H2020 Programme under Grant Agreement No.722614.

Acknowledgment

The research leading to these results has received funding from the predoctoral grant ELCOREL, which is funded by the European Union's H2020 Programme under Grant Agreement No.722614. We would like to thank Dr. M. A. Ortuño and Dr. A. J. Martin for critically discussing the results. We thank the BSC-RES for providing generous computational resources.

Table of contents

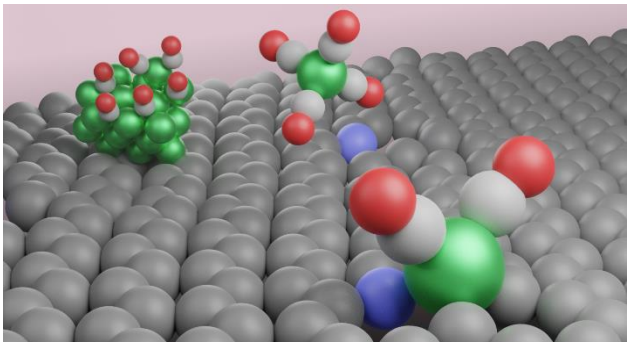

Process of Ni(211) metal surface reconstruction with eliminating $Ni(CO)_4$ and disintegrating into N-doped defect.

References

(1) Kornienko, N.; Zhao, Y.; Kley, C. S.; Zhu, C.; Kim, D.; Lin, S.; Chang, C. J.; Yaghi, O. M.; Yang, P. Metal-Organic Frameworks for Electrocatalytic Reduction of Carbon Dioxide. *J. Am. Chem. Soc.* **2015**, *137* (44), 14129–14135.

(2) Ju, W.; Bagger, A.; Hao, G. P.; Varela, A. S.; Sinev, I.; Bon, V.; Roldan Cuenya, B.; Kaskel, S.; Rossmeisl, J.; Strasser, P. Understanding Activity and Selectivity of Metal-Nitrogen-Doped Carbon Catalysts for Electrochemical Reduction of CO2. *Nat. Commun.* **2017**, *8* (1), 1–9.

(3) Tripkovic, V.; Vanin, M.; Karamad, M.; Björketun, M. E.; Jacobsen, K. W.; Thygesen, K. S.; Rossmeisl, J. Electrochemical CO2 and CO Reduction on Metal-Functionalized Porphyrin-like Graphene. *J. Phys. Chem. C* **2013**, *117* (18), 9187–9195.

(4) Li, J.; Pršlja, P.; Shinagawa, T.; Martín Fernández, A. J.; Krumeich, F.; Artyushkova, K.; Atanassov, P.; Zitolo, A.; Zhou, Y.; García-Muelas, R.; López, N.; Pérez-Ramírez, J.; Jaouen, F. Volcano Trend in Electrocatalytic Co2 Reduction Activity over Atomically Dispersed Metal Sites on Nitrogen-Doped Carbon. *ACS Catal.* **2019**, *9* (11), 10426–10439.

(5) Varela, A. S.; Ranjbar Sahraie, N.; Steinberg, J.; Ju, W.; Oh, H. S.; Strasser, P. Metal-Doped Nitrogenated Carbon as an Efficient Catalyst for Direct CO2 Electroreduction to

CO and Hydrocarbons. *Angew. Chemie - Int. Ed.* **2015**, *54* (37), 10758–10762.

(6) Varela, A. S.; Ju, W.; Bagger, A.; Franco, P.; Rossmeisl, J.; Strasser, P. Electrochemical Reduction of CO2 on Metal-Nitrogen-Doped Carbon Catalysts. *ACS Catal.* **2019**, *9* (8), 7270–7284.

(7) Möller, T.; Ju, W.; Bagger, A.; Wang, X.; Luo, F.; Ngo Thanh, T.; Varela, A. S.; Rossmeisl, J.; Strasser, P. Efficient CO2 to CO Electrolysis on Solid Ni-N-C Catalysts at Industrial Current Densities. *Energy Environ. Sci.* **2019**, *12* (2), 640–647.

(8) Zheng, T.; Jiang, K.; Ta, N.; Hu, Y.; Zeng, J.; Liu, J.; Wang, H. Large-Scale and Highly Selective CO 2 Electrocatalytic Reduction on Nickel Single-Atom Catalyst. *Joule* **2019**, *3* (1), 265–278.

(9) Jiang, K.; Siahrostami, S.; Zheng, T.; Hu, Y.; Hwang, S.; Stavitski, E.; Peng, Y.; Dynes, J.; Gangisetty, M.; Su, D.; Attenkofer, K.; Wang, H. Isolated Ni Single Atoms in Graphene Nanosheets for High-Performance CO2 Reduction. *Energy Environ. Sci.* **2018**, *11* (4), 893–903.

(10) Wen, C. F.; Mao, F.; Liu, Y.; Zhang, X. Y.; Fu, H. Q.; Zheng, L. R.; Liu, P. F.; Yang, H. G. Nitrogen-Stabilized Low-Valent Ni Motifs for Efficient CO2 Electrocatalysis. *ACS Catal.* **2020**, *10* (2), 1086–1093.

(11) Koshy, D. M.; Chen, S.; Lee, D. U.; Stevens, M. B.; Abdellah, A. M.; Dull, S. M.; Chen, G.; Nordlund, D.; Gallo, A.; Hahn, C.; Higgins, D. C.; Bao, Z.; Jaramillo, T. F. Understanding the Origin of Highly Selective CO2 Electroreduction to CO on Ni,N-Doped Carbon Catalysts. *Angewandte Chemie - International Edition*. 2020.

(12) Yang, H.; Lin, Q.; Zhang, C.; Yu, X.; Cheng, Z.; Li, G.; Hu, Q.; Ren, X.; Zhang, Q.; Liu, J.; He, C. Carbon Dioxide Electroreduction on Single-Atom Nickel Decorated Carbon Membranes with Industry Compatible Current Densities. *Nat. Commun.* **2020**, *11* (1), 1–8.

(13) Yan, C.; Li, H.; Ye, Y.; Wu, H.; Cai, F.; Si, R.; Xiao, J.; Miao, S.; Xie, S.; Yang, F.; Li, Y.; Wang, G.; Bao, X. Coordinatively Unsaturated Nickel–Nitrogen Sites towards Selective and High-Rate CO2 Electroreduction. *Energy Environ. Sci.* **2018**, *11* (5), 1204–1210.

(14) Li, X.; Bi, W.; Chen, M.; Sun, Y.; Ju, H.; Yan, W.; Zhu, J.; Wu, X.; Chu, W.; Wu, C.;

Xie, Y. Exclusive Ni-N4 Sites Realize Near-Unity CO Selectivity for Electrochemical CO2 Reduction. *J. Am. Chem. Soc.* **2017**, *139* (42), 14889–14892.

(15) Su, P.; Iwase, K.; Nakanishi, S.; Hashimoto, K.; Kamiya, K. Nickel-Nitrogen-Modified Graphene: An Efficient Electrocatalyst for the Reduction of Carbon Dioxide to Carbon Monoxide. *Small* **2016**, *12* (44), 6083–6089.

(16) Yang, H. Bin; Hung, S. F.; Liu, S.; Yuan, K.; Miao, S.; Zhang, L.; Huang, X.; Wang, H. Y.; Cai, W.; Chen, R.; Gao, J.; Yang, X.; Chen, W.; Huang, Y.; Chen, H. M.; Li, C. M.; Zhang, T.; Liu, B. Atomically Dispersed Ni(i) as the Active Site for Electrochemical CO2 Reduction. *Nat. Energy* **2018**, *3* (2), 140–147.

(17) Ma, S.; Su, P.; Huang, W.; Jiang, S. P.; Bai, S.; Liu, J. Atomic Ni Species Anchored N-Doped Carbon Hollow Spheres as Nanoreactors for Efficient Electrochemical CO2 Reduction. *ChemCatChem*. 2019, pp 6092–6098.

(18) Zhao, C.; Dai, X.; Yao, T.; Chen, W.; Wang, X.; Wang, J.; Yang, J.; Wei, S.; Wu, Y.; Li, Y. Ionic Exchange of Metal-Organic Frameworks to Access Single Nickel Sites for Efficient Electroreduction of CO2. *J. Am. Chem. Soc.* **2017**, *139* (24), 8078–8081.

(19) Yang, J.; Qiu, Z.; Zhao, C.; Wei, W.; Chen, W.; Li, Z.; Qu, Y.; Dong, J.; Luo, J.; Li, Z.; Wu, Y. In Situ Thermal Atomization To Convert Supported Nickel Nanoparticles into Surface-Bound Nickel Single-Atom Catalysts. *Angew. Chemie - Int. Ed.* **2018**, *57* (43), 14095–14100.

(20) Büchele, S.; Martín, A. J.; Mitchell, S.; Krumeich, F.; Collins, S. M.; Xi, S.; Borgna, A.; Pérez-Ramírez, J. Structure Sensitivity and Evolution of Nickel-Bearing Nitrogen-Doped Carbons in the Electrochemical Reduction of CO2. *ACS Catal.* **2020**, 3444–3454.

(21) Chen, Y.; Ji, S.; Chen, C.; Peng, Q.; Wang, D.; Li, Y. Single-Atom Catalysts: Synthetic Strategies and Electrochemical Applications. *Joule* **2018**, *2* (7), 1242–1264.

(22) Yan, C.; Li, H.; Ye, Y.; Wu, H.; Cai, F.; Si, R.; Xiao, J.; Miao, S.; Xie, S.; Yang, F.; Li, Y.; Wang, G.; Bao, X. Coordinatively Unsaturated Nickel-Nitrogen Sites towards Selective and High-Rate CO2 Electroreduction. *Energy Environ. Sci.* **2018**, *11* (5), 1204–1210.

(23) Wang, L.; Sofer, Z.; Pumera, M. Will Any Crap We Put into Graphene Increase Its

Electrocatalytic Effect? *ACS Nano* **2020**.

(24) Liu, S.; Yang, H. Bin; Hung, S. F.; Ding, J.; Cai, W.; Liu, L.; Gao, J.; Li, X.; Ren, X.; Kuang, Z.; Huang, Y.; Zhang, T.; Liu, B. Elucidating the Electrocatalytic CO2 Reduction Reaction over a Model Single-Atom Nickel Catalyst. *Angew. Chemie - Int. Ed.* **2020**, *59* (2), 798–803.

(25) Shen, J.; Kolb, M. J.; Göttle, A. J.; Koper, M. T. M. DFT Study on the Mechanism of the Electrochemical Reduction of CO2 Catalyzed by Cobalt Porphyrins. *J. Phys. Chem. C* **2016**, *120* (29), 15714–15721.

(26) Shen, J.; Kortlever, R.; Kas, R.; Birdja, Y. Y.; Diaz-Morales, O.; Kwon, Y.; Ledezma-Yanez, I.; Schouten, K. J. P.; Mul, G.; Koper, M. T. M. Electrocatalytic Reduction of Carbon Dioxide to Carbon Monoxide and Methane at an Immobilized Cobalt Protoporphyrin. *Nat. Commun.* **2015**, *6* (1), 8177.

(27) Chen, Z.; Mitchell, S.; Vorobyeva, E.; Leary, R. K.; Hauert, R.; Furnival, T.; Ramasse, Q. M.; Thomas, J. M.; Midgley, P. A.; Dontsova, D.; Antonietti, M.; Pogodin, S.; López, N.; Pérez-Ramírez, J. Stabilization of Single Metal Atoms on Graphitic Carbon Nitride. *Adv. Funct. Mater.* **2017**, *27* (8), 1605785.

(28) Kresse, G.; Furthmüller, J. Efficiency of Ab-Initio Total Energy Calculations for Metals and Semiconductors Using a Plane-Wave Basis Set. *Comput. Mater. Sci.* **1996**, *6* (1), 15–50.

(29) Joubert, D. From Ultrasoft Pseudopotentials to the Projector Augmented-Wave Method. *Phys. Rev. B - Condens. Matter Mater. Phys.* **1999**, *59* (3), 1758–1775.

(30) Perdew, J. P.; Burke, K.; Ernzerhof, M. Generalized Gradient Approximation Made Simple. *Phys. Rev. Lett.* **1996**, *77* (18), 3865–3868.

(31) Grimme, S.; Antony, J.; Ehrlich, S.; Krieg, H. A Consistent and Accurate Ab Initio Parametrization of Density Functional Dispersion Correction (DFT-D) for the 94 Elements H-Pu. *J. Chem. Phys.* **2010**, *132* (15).

(32) Blöchl, P. E. Projector Augmented-Wave Method. *Phys. Rev. B* **1994**, *50* (24), 17953–17979.

(33) Pack, J. D.; Monkhorst, H. J. "special Points for Brillouin-Zone Integrations"-a Reply. *Phys. Rev. B* **1977**, *16* (4), 1748–1749.

(34) Barmparis, G. D.; Lodziana, Z.; Lopez, N.; Remediakis, I. N. Nanoparticle Shapes by Using Wulff Constructions and First-Principles Calculations. *Beilstein J. Nanotechnol.* **2015**, *6* (1), 361–368.

(35) Wulff, G. XXV. Zur Frage Der Geschwindigkeit Des Wachsthums Und Der Auflösung Der Krystallflächen. *Zeitschrift für Krist. - Cryst. Mater.* **1901**, *34* (1), 449–530.

(36) Momma, K.; Izumi, F. VESTA 3 for Three-Dimensional Visualization of Crystal, Volumetric and Morphology Data. *J. Appl. Crystallogr.* **2011**, *44* (6), 1272–1276.

(37) Barmparis, G. D.; Remediakis, I. N. Dependence on CO Adsorption of the Shapes of Multifaceted Gold Nanoparticles: A Density Functional Theory. *Phys. Rev. B - Condens. Matter Mater. Phys.* **2012**, *86* (8), 1–7.

(38) Loffreda, D.; Simon, D.; Sautet, P. Dependence of Stretching Frequency on Surface Coverage and Adsorbate-Adsorbate Interactions: A Density-Functional Theory Approach of CO on Pd(111). *Surf. Sci.* **1999**, *425* (1), 68–80.

(39) Peterson, A. A.; Abild-Pedersen, F.; Studt, F.; Rossmeisl, J.; Nørskov, J. K. How Copper Catalyzes the Electroreduction of Carbon Dioxide into Hydrocarbon Fuels. *Energy Environ. Sci.* **2010**, *3* (9), 1311–1315.

(40) Nørskov, J. K.; Rossmeisl, J.; Logadottir, A.; Lindqvist, L.; Kitchin, J. R.; Bligaard, T.; Jónsson, H. Origin of the Overpotential for Oxygen Reduction at a Fuel-Cell Cathode. *J. Phys. Chem. B* **2004**, *108* (46), 17886–17892.

(41) Chan, K.; Tsai, C.; Hansen, H. A.; Nørskov, J. K. Molybdenum Sulfides and Selenides as Possible Electrocatalysts for CO 2 Reduction. *ChemCatChem* **2014**, *6* (7), 1899–1905.

(42) Garcia-Ratés, M.; López, N. Multigrid-Based Methodology for Implicit Solvation Models in Periodic DFT. *J. Chem. Theory Comput.* **2016**, *12* (3), 1331–1341.

(43) Reda, M.; Hansen, H. A.; Vegge, T. DFT Study of Stabilization Effects on N-Doped Graphene for ORR Catalysis. *Catal. Today* **2018**, *312* (December 2017), 118–125.

(44) Álvarez-Moreno, M.; De Graaf, C.; López, N.; Maseras, F.; Poblet, J. M.; Bo, C. Managing the Computational Chemistry Big Data Problem: The IoChem-BD Platform. *J. Chem. Inf. Model.* **2015**, *55* (1), 95–103.

(45) P.Prslja. https://iochem-bd.iciq.es/browse/review-collection/100/23937/2c9caed863ab2d67380cb461.

(46) Beley, M.; Collin, J.-P.; Ruppert, R.; Sauvage, J.-P. Electrocatalytic Reduction of CO2 by Ni Cyclam2+ in Water: Study of the Factors Affecting the Efficiency and the Selectivity of the Process. *ChemInform* **1987**, *18* (14), 7461–7467.

(47) Millet, M.-M.; Algara-Siller, G.; Wrabetz, S.; Mazheika, A.; Girgsdies, F.; Teschner, D.; Seitz, F.; Tarasov, A.; Levchenko, S. V; Schlögl, R.; Frei, E. Ni Single Atom Catalysts for CO2 Activation. *J. Am. Chem. Soc.* **2019**, *141* (6), 2451–2461.

(48) Li, Q.; Rellán-Piñeiro, M.; Almora-Barrios, N.; Garcia-Ratés, M.; Remediakis, I. N.; López, N. Shape Control in Concave Metal Nanoparticles by Etching. *Nanoscale* **2017**, *9* (35), 13089–13094.

(49) Voorhees, P. W. The Theory of Ostwald Ripening. *J. Stat. Phys.* **1985**, *38* (1), 231–252.

(50) Ouyang, R.; Liu, J. X.; Li, W. X. Atomistic Theory of Ostwald Ripening and Disintegration of Supported Metal Particles under Reaction Conditions. *J. Am. Chem. Soc.* **2013**, *135* (5), 1760–1771.

(51) Berkó, A.; Solymosi, F. Adsorption-Induced Structural Changes of Rh Supported by TiO2(110)-(1×2): An STM Study. *J. Catal.* **1999**, *183* (1), 91–101.